ACS OMEGA

Article

Cite This: ACS Omega 2018, 3, 2699−2705

Biomimetic Synthesis of Polydopamine Coated $ZnFe_2O_4$ Composites as Anode Materials for Lithium-Ion Batteries

Hongyun Yue,[†,§,∥] Ting Du,[†,∥] Qiuxian Wang,[§,∥] Zhenpu Shi,[†,∥] Hongyu Dong,[†,§,∥] Zhaoxia Cao,[†,§,∥] Yun Qiao,[†,§,∥] Yanhong Yin,[†,§,∥] Ruimin Xing,*[,‡] and Shuting Yang*[,†,§,∥]

[†]School of Chemistry and Chemical Engineering, Henan Normal University, Xinxiang 453007, Henan, P. R. China

[‡]Henan Key Laboratory of Polyoxometalate Chemistry, Institute of Molecular and Crystal Engineering, College of Chemistry and Chemical Engineering, Henan University, Kaifeng 475001, P. R. China

[§]Collaborative Innovation Center of Henan Province for Motive Power and Key Materials, Henan Battery Research Institute, Xinxiang 453007, P. R. China

[∥]National and Local Joint Engineering Laboratory of Motive Power and Key Materials, Xinxiang 453007, Henan, P. R. China

Supporting Information

ABSTRACT: Metal oxides as anode materials for lithium storage suffer from poor cycling stability due to their conversion mechanisms. Here, we report an efficient biomimetic method to fabricate a conformal coating of conductive polymer on $ZnFe_2O_4$ nanoparticles, which shows outstanding electrochemical performance as anode material for lithium storage. Polydopamine (PDA) film, a bionic ionic permeable film, was successfully coated on the surfaces of $ZnFe_2O_4$ particles by the self-polymerization of dopamine in the presence of an alkaline buffer solution. The thickness of PDA coating layer was tunable by controlling the reaction time, and the obtained $ZnFe_2O_4$/PDA sample with 8 nm coating layer exhibited an outstanding electrochemical performance in terms of cycling stability and rate capability. $ZnFe_2O_4$/PDA composites delivered an initial discharge capacity of 2079 mAh g^{-1} at 1 A g^{-1} and showed a minimum capacity decay after 150 cycles. Importantly, the coating layer improved the rate capability of composites compared to that of its counterpart, the bare $ZnFe_2O_4$ particle materials. The outstanding electrochemical performance was because of the buffering and protective effects of the PDA coating layer, which could be a general protection strategy for electrode materials in lithium-ion batteries.

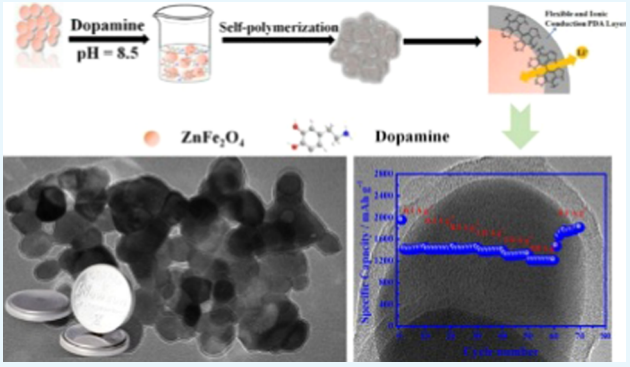

INTRODUCTION

Lithium-ion batteries (LIBs) have been widely applied to electronic devices, electric vehicles (EVs), and hybrid electric vehicles.[1] LIBs have become increasingly popular and have attracted tremendous attention in the past decades.[2,3] The increasing demands for high-performance LIBs have motivated significant research in exploring low-cost and high-performance electrode materials. Otherwise, anode materials are key ingredients of LIBs.[4,5] Nowadays, commercial graphite has been used as the anode material in LIBs. However, it suffers from low theoretical capacity (372 mAh g^{-1}) and fast capacity fading, especially at higher current rates, which hinder the increasing demands of LIBs for EVs and other higher power applications.[4,6] Therefore, it is vitally necessary to develop anode materials with high capacity, steady cycling, and rate performance.[7]

To overcome these challenges, many studies focused on the electrochemical Li-storage properties of ternary mixed transition metal oxides (TMOs), including $MeMn_2O_4$ (Me = Fe, Mg, Zn, Cu), $MeCo_2O_4$ (Me = Zn, Co, and Ni), and $MeFe_2O_4$ (Me = Co, Ni, Cu, and Zn).[8−12] Among these ternary mixed TMOs, $MeFe_2O_4$ attract more attention as iron is cheaper, more abundant, and environmental friendly. Among all of the candidates, $ZnFe_2O_4$ attracts the most attention owing to its low cost, easy preparation, and high theoretical capacity (1000.5 mAh g^{-1}). However, $ZnFe_2O_4$ anode materials greatly suffer from fast capacity fading and poor rate capability arising from their low electronic conductivity and large volume expansion in the lithiation−delithiation process, which is related to its conversion reaction mechanism during charge−discharge cycles.[13−15] Much effort has been dedicated to overcoming these pulverization problems, such as introducing conductive agents and constructing nanostructures.[16,17] Among these various methods, carbon coating has been widely recognized as an effective approach to improve the electrochemical performance of $ZnFe_2O_4$ particles. The carbon

Received: November 8, 2017
Accepted: January 29, 2018
Published: March 7, 2018

DOI: 10.1021/acsomega.7b01752
ACS Omega 2018, 3, 2699−2705

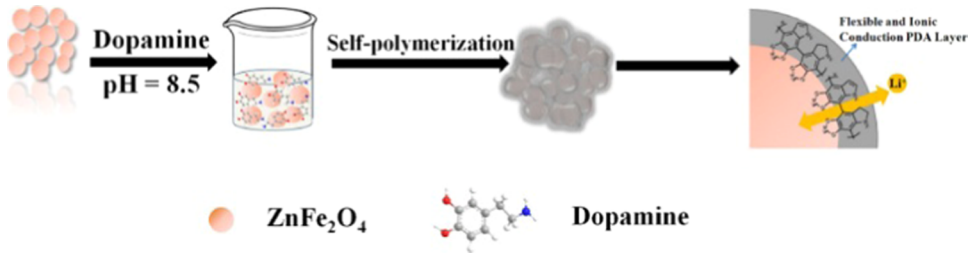

Figure 1. Schematic illustration for the fabrication of ZFDA1.

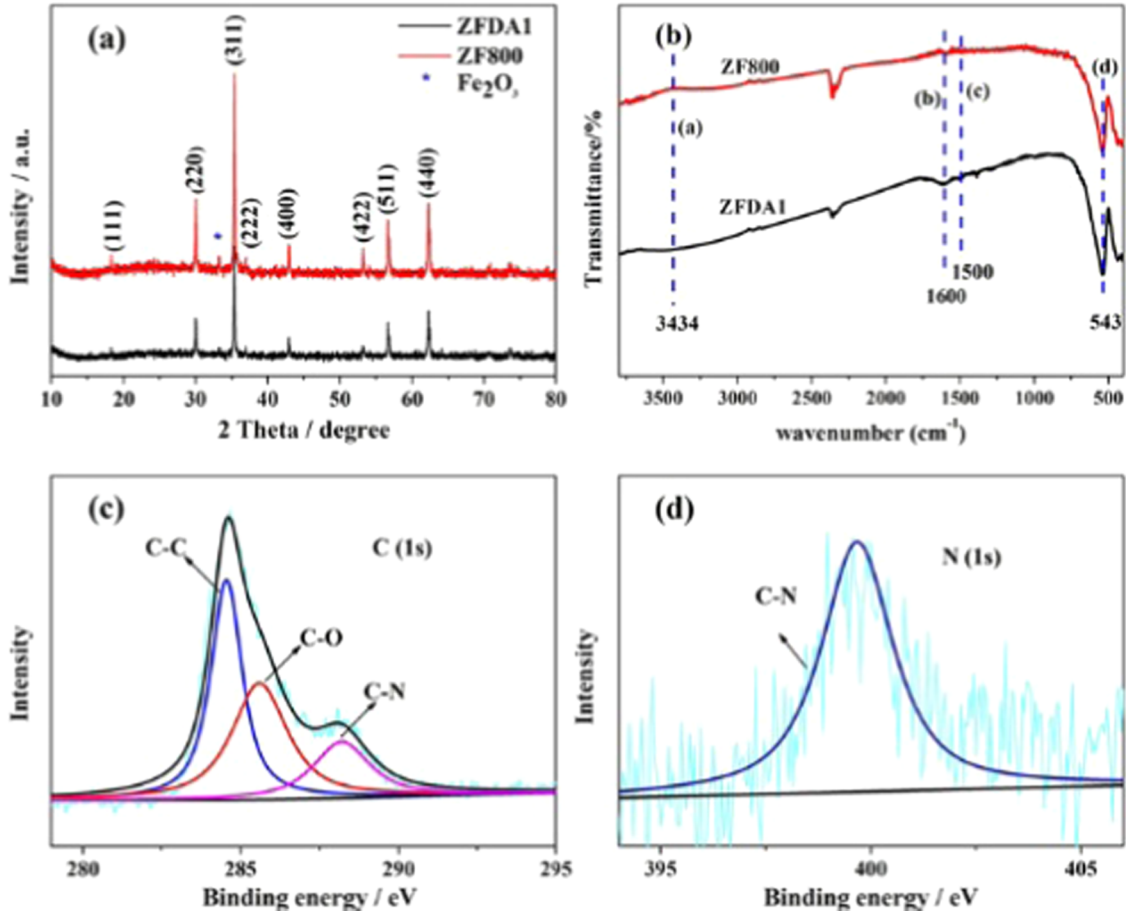

Figure 2. XRD patterns of ZF800 and ZFDA1 (a), Fourier transform infrared (FTIR) spectra of ZF800 and ZFDA1 (b), and X-ray photoelectron spectroscopy (XPS) survey spectra of C 1s and N 1s for ZFDA1 composites (c) and (d).

coating layer can improve the electronic conductivity of $ZnFe_2O_4$ materials and simultaneously accommodate the strain of volume change during the charge/discharge process, which ensure their structural integrity and improve their cycling stability.[18−23] Moreover, the coating protection of $ZnFe_2O_4$ materials can dramatically decrease the surface energy of $ZnFe_2O_4$ particles, which could mitigate the side reactions between the electrode and electrolyte.[24] However, despite the above-mentioned advantages, it is difficult to fabricate a conformal carbon coating layer on $ZnFe_2O_4$ materials, which usually needs pyrolysis and chemical vapor deposition processes.[25]

Marine mussels exhibit highly strong adhesion to a wide variety of organic and inorganic substances. The affinity of marine mussels to their substances is mainly associated with adhesive proteins containing abundant catecholamine. Dopamine, a mussel-inspired adhesion material containing both catechol and amine groups, can be polymerized at mild basic pH to form an adhesive polymer polydopamine (PDA) film on a wide range of substrates. The PDA film plays an important role in surface science.[26,27] Besides the adhesive property, the PDA film has good ionic permeability, which allows the ions penetrate through the film, which could be used for modifying electrode materials for LIBs. The PDA-modified separators can improve the wetting ability, the electrolyte uptake, and the ionic conductivity. PDA has been used to modify the sulfur cathode in Li/S battery and CuO, SnO_2, Si, and Ti−Si alloy anode materials for lithium-ion batteries.[26−30] PDA coating layer can effectively improve their electrochemical performances.

Herein, novel $ZnFe_2O_4$/PDA composites were successfully synthesized through a facile sol−gel synthesis and an in situ polymerization approach. The obtained $ZnFe_2O_4$/PDA composites exhibited very high reversible capacity, excellent rate capability, and outstanding cycling stability. $ZnFe_2O_4$/PDA

DOI: 10.1021/acsomega.7b01752
ACS Omega 2018, 3, 2699−2705

composites delivered an initial discharge capacity of 2079 mAh g^{-1} at 1 A g^{-1} and retained a reversible discharge capacity of 2074 mAh g^{-1} after 150 cycles. More importantly, $ZnFe_2O_4$/PDA electrode showed an excellent rate capability, which exhibited a reversible discharge capacity of 1187 mAh g^{-1} at 5 A g^{-1}.

RESULTS AND DISCUSSION

The fabrication process of ZFDA1 composite is illustrated in Figure 1, which mainly consists of two processes. First, ZF800 was synthesized by sol−gel method. Subsequently, PDAs were homogeneously coated on the surface of ZF800 by the self-polymerization of dopamine in the presence of buffer solution. The obtained ZFDA1 delivered the most optimal electrochemical performance compared to that of the ZFDA2, ZFDA3, and ZFDA4 electrodes. Detailed information of the structure, morphology, coating layer, and electrochemical performances of ZFDA2, ZFDA3, and ZFDA4 samples is presented in Supporting Information Figures S1−S3. Figure 2a shows the X-ray diffraction (XRD) patterns of ZF800 and ZFDA1 samples. Most of the observed diffraction peaks were well consistent with cubic spinel $ZnFe_2O_4$ (JCPDS card no. 22-1012, space group *Fd3m*, space group no. 227). Compared to the XRD pattern of ZF800, the pattern of ZFDA1 showed a decrease in peak intensity due to the presence of the PDA layer on the crystal. Obviously, the diffraction peaks at 2θ values of 18.24, 30.0, 35.34, 36.97, 42.95, 47.03, 53.28, and 56.79° could be associated with the reflections obtained from (111), (220), (311), (222), (400), (331), (422), and (511) planes of the ZF800 and ZFDA1 samples. The strong intensity and narrow peak width of diffraction peaks indicated that the samples were well crystallized. In addition, the ZF800 and ZFDA1 samples showed some small impurity peaks (Figure 2a), which were well matched with Fe_2O_3 (JCPDS card no. 84-0307). The Fe_2O_3 peaks appeared with the increasing calcination temperature of $ZnFe_2O_4$.

FTIR was carried out to examine the surface functional groups of the ZF800 and ZFDA1 samples. As shown in Figure 2b, both ZFDA1 and ZF800 samples exhibited strong characteristic peaks at 543 cm^{-1}, which should be attributed to the vibration of the Zn−O bond. The absorption peak of Zn−O bond in ZFDA1 was weaker than that of ZF800, which was related to the PDA coating layer. In the spectrum of ZFDA1, two peaks at 1500 and 1600 cm^{-1} appeared, which were due to the aromatic rings in the PDA layer.[32−35] Compared to those of the ZF800 samples, absorption peaks of ZFDA1 at 3434 cm^{-1} are broad, which was ascribed to the stretching vibration absorption of −NH groups linked to the composites.[36] These results clearly suggested that the PDA conductive polymer was successfully coated on the surface of $ZnFe_2O_4$.

The polymer coating layer of ZFDA1 was further characterized by XPS. As shown in Figure 2c,d, the C 1s XPS of PDA is presented in Figure 2c. The peaks at binding energies of 284.5, 285.4, and 288.1 eV were consistent with the nonoxygenated carbon C−C, carbon in C−O, and C−N.[37,38] In addition, Figure 2d shows the peak centered at 399.6 eV, which was associated with C−N.[36] These features were all typical peak positions of PDA. The survey spectrum indicated the presence of PDA coating layer, which was in good accordance with the result of FTIR (Figure 2b).

The surface morphologies of ZF800 and ZFDA1 composites are shown in Figure 3. The average crystallite sizes of the

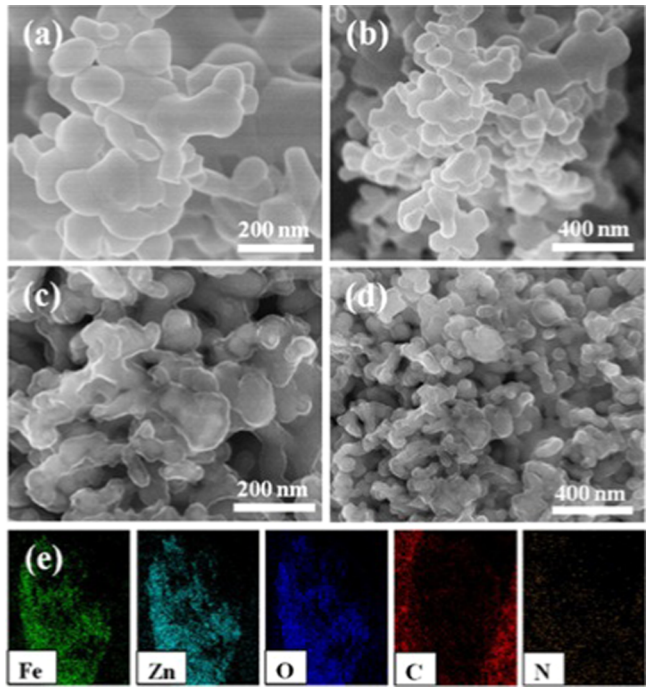

Figure 3. Field emission scanning electron microscope (FESEM) images of ZF800 (a, b) and ZFDA1 (c, d), and energy-dispersive X-ray spectroscopy (EDS) mapping images of ZFDA1 (e).

compounds were 100−200 nm. The morphologies of ZF800 particles were similar to those of ZFDA1 composites (Figure 3a,b). Compared to those of the ZF800 samples, the particles of ZFDA1 were wrapped by homogenous and continuous PDA layer. PDA had high affinity to $ZnFe_2O_4$ particles and played a significant role in forming a homogenous and continuous PDA layer. The high affinity of PDA was associated with its catechol group, which can coordinate with Fe element in $ZnFe_2O_4$.[39] In addition, the element mapping images presented a uniform distribution of Fe, Zn, O, C, and N elements in the ZFDA1 composites, which revealed that PDA was well coated on the surface of ZF800.

The microstructures of ZF800 samples and ZFDA1 composites were further investigated by transmission electron microscopy (TEM) observation, and the results are shown in Figure 4. It was confirmed that the ZF800 samples were embedded in the homogenous and continuous PDA layer and the thickness of the PDA layer was about 8 nm, which was in accordance with the results of FESEM images (Figure 3c,d). Figure 4e shows that the values of interplanar spacing of the ordered crystallites structure were 0.254 and 0.298 nm, which corresponded well with the (311) and (220) crystal planes of $ZnFe_2O_4$ particles (JCPDS card no. 22-1012).

The electrochemical behavior of lithium ion with the obtained ZF800 and ZFDA1 as electrodes was investigated at a current density of 1 A g^{-1}, and the results are shown in Figure 5a. The ZFDA1 electrode exhibited initial charge and discharge capacities of 1438.6 and 2079 mAh g^{-1}, respectively, which were higher than those of the ZF800 electrode. The discharge capacity of the ZFDA1 electrode slowly decreased to 1407.4 mAh g^{-1} in the initial eight cycles, whereas for the ZF800 electrode it decreased to 1160.5 mAh g^{-1}. Noticeably, the capacities of both ZFDA1 and ZF800 slightly increased to 1807.9 and 1540.2 mAh g^{-1} at the 100th cycle, respectively, which should be due to the wettability of the electrodes. After

DOI: 10.1021/acsomega.7b01752
ACS Omega 2018, 3, 2699−2705

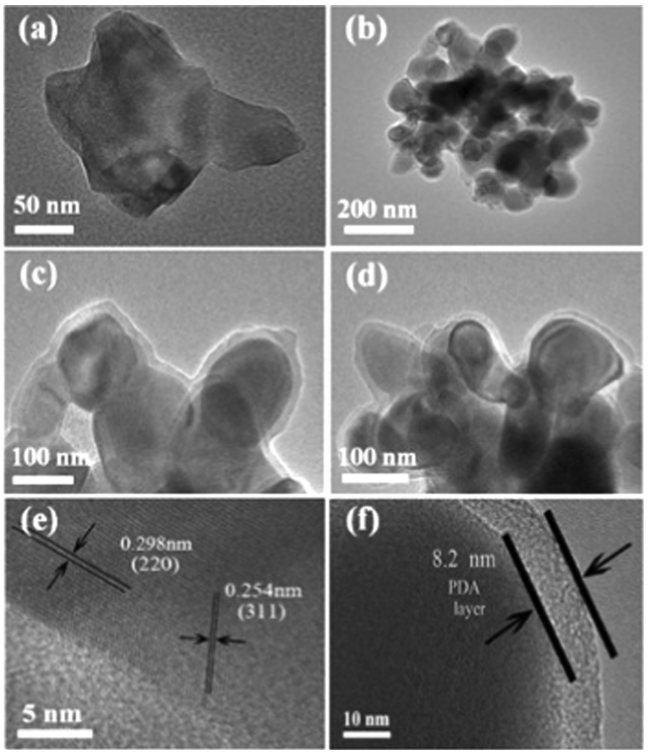

Figure 4. TEM images of ZF800 (a, e) and ZFDA1 (b–d, and f).

150 charging/discharging cycles, the ZFDA1 electrode reached a discharge capacity of 2074 mAh g^{-1} and no apparent capacity decay was observed. In contrast, the ZF800 electrode began to show capacity decay after 100 cycles. Clearly, the electrochemical performance of ZFDA1 composite was superior to that of ZF800. This result confirmed that the particles dispersed and embedded well in the PDA coating layer, which could buffer the volume changes of the active materials during electrochemical cycling, resulting in the improvement of electrochemical performance and cycle life.[26,27]

The rate performances of ZF800 and ZFDA1 electrodes were further tested at different current densities. As shown in Figure 5b, the ZFDA1 electrode showed higher reversible capacities than did the ZF800 electrode with the current density ranging from 0.1 to 5 A g^{-1}. The ZFDA1 electrode delivered discharge capacities of 1441.7, 1418, 1429.8, 1390.6, 1313.7, and 1215.3 mAh g^{-1}. At the higher current density of 5 A g^{-1}, the ZFDA1 electrode also maintained a capacity of 1215.3 mAh g^{-1}, which was much higher than that of the ZF800 electrode (1015.6 mAh g^{-1}). Subsequently, the current density reduced to 0.1 A g^{-1}, the ZFDA1 electrode recovered the capacity of 1722.7 mAh g^{-1} at the 70th cycle, and the ZF800 electrode was 1544.8 mAh g^{-1}. The superior rate performance of ZFDA1 should be ascribed to PDA coating layer. The existence of the catechol and amine polar groups of the PDA increased electrolyte wetting and enhanced ionic conductivity of the electrode.[26,40] Clearly, the PDA coating layer played a key role in improving rate performance.

Figure 6a,b shows the charge/discharge curves of ZF800 and ZFDA1 electrodes for the first, second, third, fourth, and fifth cycles at the current density of 1 A g^{-1} between 0.005 and 3 V. The initial capacity loss was mainly caused by the formation of the solid electrolyte interface and the irreversible reaction on the electrode surface.[24,36] During the initial lithiation process, there was a voltage plateau located at 0.86 V, which was due to the phase transition from $ZnFe_2O_4$ to $Li_xZnFe_2O_4$ ($x \sim 0.5$).[41] Furthermore, two plateaus at about 0.7 and 0.4 V for the ZFDA1 electrode and at 0.7 V for the ZF800 electrode were due to the reduction of Fe^{2+} and Zn^{2+} to metallic states during the formation of Li–Zn alloys and Li_2O,[24,42−44] which were in good agreement with the results of cyclic voltammetry (CV) measurement.

To further investigate the electrochemical properties of ZFDA1 and ZF800 during the cycling process, CV measurements were first performed. Figures 6c and 7 show the CV curves of ZFDA1 for the first three cycles at a scan rate of 0.1 mV s^{-1} in the potential ranging from 0.005 to 3 V. It was clear that the initial cathodic peak was obviously different from that of the subsequent cycles. During the first cathodic sweep of ZFDA1, one small reduction peak could be observed at about 0.86 V, which usually originated from Li intercalation into $ZnFe_2O_4$ to form the intercalation phase, $Li_xZnFe_2O_4$.[41] Other reduction peaks centered at about 0.7 and 0.4 V for the ZFDA1 electrode were due to the reduction of Fe^{2+} and Zn^{2+} to metallic states during the formation of Li–Zn alloys and Li_2O.[24,42−44] In the subsequent cycles, these cathodic peaks shifted to about 0.9 V, which was in accordance with the reversible lithium storage associated with the reversible reduction of ZnO and Fe_2O_3 to metal particles embedded in Li_2O.[43] Furthermore, the initial anodic potential peak locating

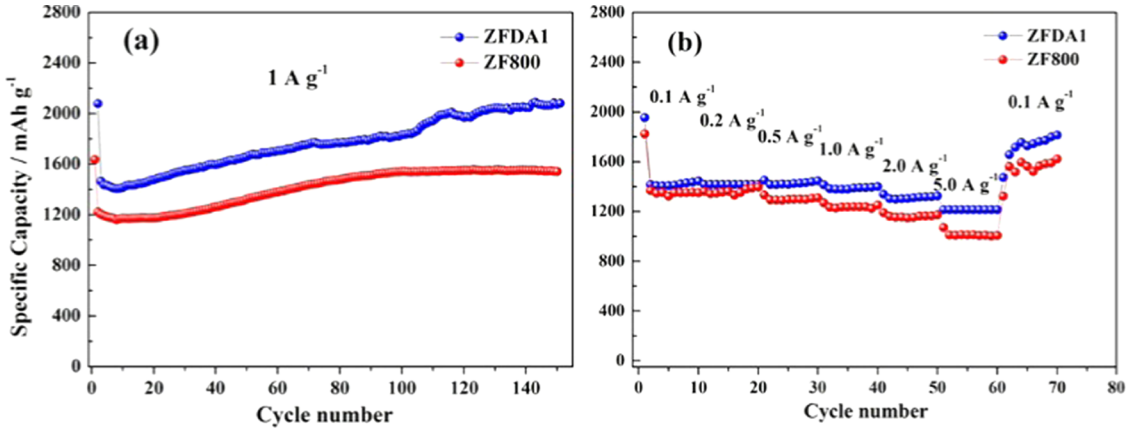

Figure 5. Cycling performances of ZF800 and ZFDA1 electrodes at the current density of 1 A g^{-1} (a) and rate capabilities of ZF800 and ZFDA1 electrodes (b).

DOI: 10.1021/acsomega.7b01752
ACS Omega 2018, 3, 2699−2705

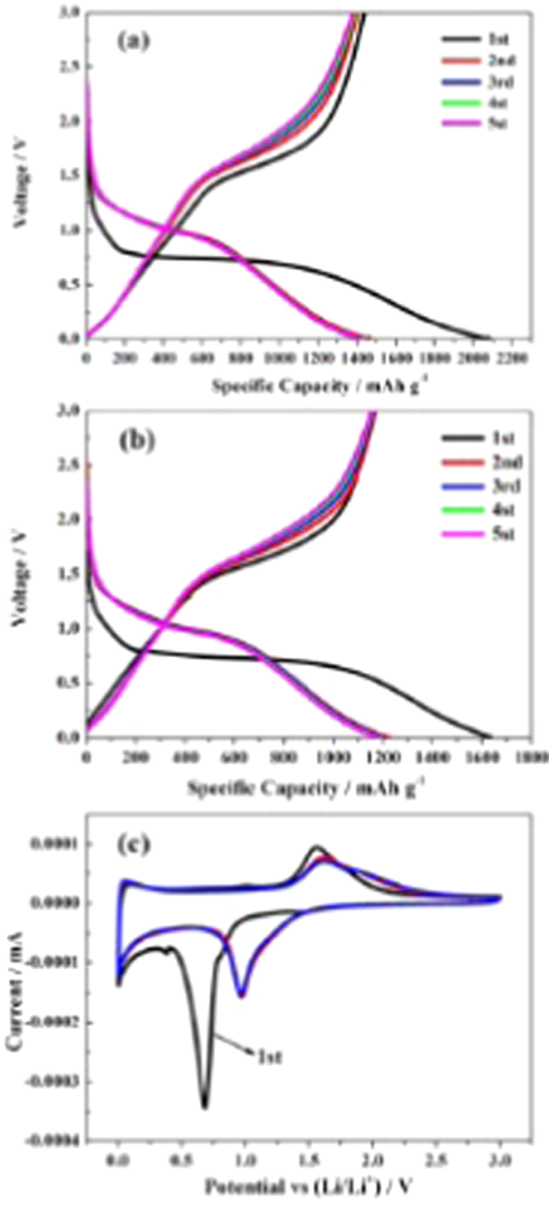

Figure 6. Voltage profiles of ZFDA1 (a) and ZF800 (b) for the first, second, third, fourth, and fifth cycles at the current density of 1 A g^{-1}, and CV curves of ZFDA1 for the first three cycles at 0.1 mV s^{-1} between 0.005 and 3 V (c).

at about 1.58 V was attributed to the oxidation of Fe^0 and Zn^0 to Fe_2O_3 and ZnO.[41] The CV curves did not change significantly on the further sweeps, suggesting the good cycling stability of ZFDA1.

The enhanced electrochemical performance of the ZFDA1 electrode was further supported by EIS measurements from 10^{-1} to 10^5 after 50 cycles. The Nyquist plots all consisted of a depressed semicircle in high-medium-frequency range and an inclined line in the low-frequency region. The semicircle related to the charge transfer resistance (R_{ct}) of the electrode system and the electrolyte resistance (R_e). The inclined line was derived from the Warburg impedance (Z_w) corresponding to the lithium-ion diffusion in electrode materials.[24,39,43] The radius of the semicircle barely changed for both electrodes. As observed from the slope of the inclined line, the impedance of the ZF800 electrode was significantly higher than that of the

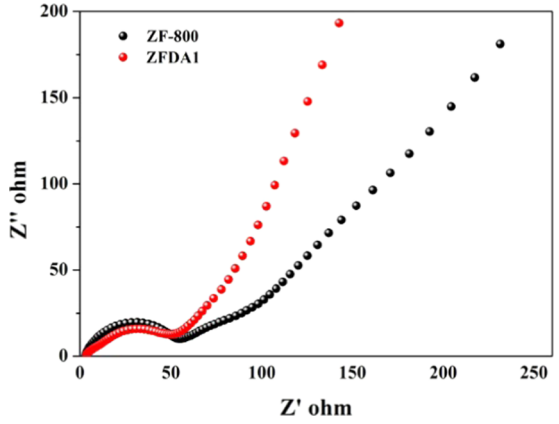

Figure 7. Electrochemical impedance spectra of ZF800 particles and ZFDA1 composites; the electrochemical impedance spectroscopy (EIS) were recorded after 50 cycles.

ZFDA1 electrode. These evidences demonstrated that the PDA layer would not decrease the transportation of Li ions and generate a lower diffusion resistance during continuous charge/discharge processes.

CONCLUSIONS

In summary, a novel approach to fabricate a functional PDA coating layer was developed to accommodate the volume expansion through a facile and biomimetic method. It was a simple and low-cost method of synthesizing a uniform bionic ionic permeable PDA film coated on $ZnFe_2O_4$. Compared with the methods using carbonized polymers, this method is simple and energy-saving, which has good potential in the large-scale application of high-capacity electrode materials. The $ZnFe_2O_4$ with PDA coating exhibited initial charge and discharge capacities of 1438.6 and 2079 mAh g^{-1}, respectively. After charging/discharging cycle for 150 cycles at the current density of 1 A g^{-1}, the electrode still maintained a discharge capacity as high as 2074 mAh g^{-1}. More importantly, the conductive polymer coating of $ZnFe_2O_4$ significantly improved the rate capability at high current densities. The excellent electrochemical performance is believed to be ascribed to the homogenous and continuous PDA coating, which could accommodate the volume change. The rational designed materials showed an outstanding performance as anode for LIBs, and this biomimetic method could be a general protection method for electrode materials for LIBs.

EXPERIMENTAL SECTION

Chemicals. All of the chemicals used in this experiment were analytical grade without any further purification. $Zn(NO_3)_2{\cdot}6H_2O$ and dopamine hydrochloride were provided by Aladdin Reagent Co. Ltd. (Shanghai, China). $Fe(NO_3)_3{\cdot}9H_2O$ and glycine were purchased from Tianjin Denn Chemical Reagent Co. Ltd. and Huzhou Biological Chemical Co. Ltd., respectively. Tris(hydroxymethyl)aminomethane hydrochloride (Tris-HCl) was provided by Sinopharm Chemical Reagent Co. Ltd.

Synthesis of $ZnFe_2O_4$ Particles. In a typical sol−gel synthesis, 10 mmol $Zn(NO_3)_2{\cdot}6H_2O$, 20 mmol $Fe(NO_3)_3{\cdot}9H_2O$, and 60 mmol glycine were dissolved in 40 mL of distilled water. Then, the sample was kept at 60 °C with constant magnetic stirring for 12 h to form bronzing gel. Subsequently, the resulting bronzing gel was transferred into a

DOI: 10.1021/acsomega.7b01752
ACS Omega 2018, 3, 2699−2705

muffle furnace and treated at 100 °C to obtain the bulk precursor. Finally, the obtained bulk precursor was calcined in a tube furnace under air atmosphere at 160 °C for 2 h at a heating rate of 10 °C min^{-1} and then at 800 °C for 2 h at a heating rate of 5 °C min^{-1}. The obtained $ZnFe_2O_4$ was called ZF800.

Synthesis of $ZnFe_2O_4$/PDA Composite. First, 200 mg of $ZnFe_2O_4$ particles and 40 mg of dopamine hydrochloride were dispersed into 20 mL of tris(hydroxymethyl)aminomethane hydrochloride (Tris-HCl, pH 8.5). The above-mentioned four same mixtures were stirred for 2, 4, 6, and 10 h at room temperature. The obtained composites were washed three times by deionized water and dried at 80 °C for 12 h. The samples stirred for 2, 4, 6, and 10 h were denoted ZFDA1, ZFDA2, ZFDA3, and ZFDA4, respectively.

Characterizations. The crystal structures of ZFDA1 and ZF800 were characterized with X-ray diffraction (XRD) with the 2θ range of 10−80°, which were performed by Bruker D8 Advance using Cu Kα radiation (λ = 0.1541 nm). The morphologies of all of the samples were determined using field emission scanning electron microscopy (FESEM, JSM-6700F). The element composition was observed using energy dispersive spectroscopy (EDS). The crystal structure details were further determined using transition electron microscopy (TEM); the TEM images were collected by JEOL JEM-2100 microscope with an accelerating voltage of 200 kV. X-ray photoelectron spectroscopy (XPS) analysis was performed by Kratos Axis Ultra spectroscopy with a monochromatic Al Kα radiation ($h\nu$ = 1486.6 eV). FTIR spectra of the materials were recorded on the Fourier transform infrared (FTIR) spectrometer (Themo Nicole 670FT-IR).

Electrochemical Measurements. To test the electrochemical performance, the samples were mixed with super-P and sodium alginate solution at the mass ratio of 4:4:2 in distilled water to form homogenous slurry by ball-milling for 12 h. The slurry was pasted onto a copper foil and then dried at 60 °C for 12 h in a vacuum oven. Subsequently, the obtained electrode was punched to circle plates with the diameter of 12 mm, whose mass loading was about 1.6 mg cm^{-2}, close to that in another study.[31] CR 2032 coin-type cells were assembled in an argon-filled glovebox. The pure Li metal was used as the counter electrode and microporous membrane was used as a separator. The electrolyte used here was 1.0 mol L^{-1} $LiPF_6$ in a mixed solvent of ethylene carbonate and dimethyl carbonate (1:1 by v/v). The galvanostatic discharging−charging measurements and rate capability of the test cells were tested using a LAND Cell test system (CT2001A, Wuhan, China) at 0.005−3.0 V (vs Li/Li^+). Cyclic voltammetry (CV) and electrochemical impedance spectroscopy (EIS) of the cells were conducted using a Solartron Analytical electrochemical workstation. The EIS data were recorded at the frequency range from 0.1 Hz to 100 kHz with an alternating current voltage amplitude of 10 mV.

■ ASSOCIATED CONTENT

Supporting Information

The Supporting Information is available free of charge on the ACS Publications website at DOI: 10.1021/acsomega.7b01752.

XRD patterns of ZFDA2, ZFDA3, and ZFDA4; FESEM images of ZFDA2, ZFDA3, and ZFDA4; and cycling/rate performances of ZFDA2, ZFDA3, and ZFDA4 electrodes (PDF)

■ AUTHOR INFORMATION

Corresponding Authors

*E-mail: xingenjoy@163.com (R.X.).
*E-mail: shutingyang@foxmail.com (S.Y.).

ORCID

Zhaoxia Cao: 0000-0002-0333-2022
Yun Qiao: 0000-0001-8016-1557
Shuting Yang: 0000-0001-7841-0016

Notes

The authors declare no competing financial interest.

■ ACKNOWLEDGMENTS

This work was financially supported by the National Nature Science Foundation of China (Nos. U1504211, 21501049, 21471049, and 51502082), the Key Project of Science and Technology Department of Henan Province (Nos. 142102210449 and 142102210452), and the Key Project of Science and Technology of Henan Educational Committee, China (No. 14B150007).

■ REFERENCES

(1) Tarascon, J. M.; Armand, M. Hydrogen-storage materials for mobile applications. *Nature* **2001**, *414*, 359−367.
(2) Goodenough, J. B.; Kim, Y. Challenges for Rechargeable Li Batteries. *Chem. Mater.* **2010**, *22*, 587−603.
(3) Armand, M.; Tarascon, J. M. Researchers must find a sustainable way of providing the power our modern lifestyles demand. *Nature* **2008**, *451*, 652−657.
(4) Goodenough, J. B.; Park, K. S. The Li-Ion Rechargeable Battery: A Perspective. *J. Am. Chem. Soc.* **2013**, *135*, 1167−1176.
(5) Dunn, B.; Kamath, H.; Tarascon, J. M. Electrical energy storage for the grid: a battery of choices. *Science* **2011**, *334*, 928−935.
(6) Yuan, C.; Wu, H. B.; Xie, Y.; Lou, X. W. Mixed Transition-Metal Oxides: Design, Synthesis, and Energy-Related Application. *Angew. Chem., Int. Ed.* **2014**, *53*, 1488−1504.
(7) Bruce, P. G.; Scrosati, B.; Tarascon, J. M. Nanomaterials for Rechargeable Lithium Batteries. *Angew. Chem., Int. Ed.* **2008**, *47*, 2930−2946.
(8) Zhang, G.; Yu, L.; Wu, H. B.; Hoster, H. E.; Lou, X. W. Formation of $ZnMn_2O_4$ Ball-in-Ball Hollow Microspheres as a High-Performance Anode for Lithium-Ion Batteries. *Adv. Mater.* **2012**, *24*, 4609−4613.
(9) Liu, B.; Zhang, J.; Wang, X.; Chen, G.; Chen, D.; Zhou, C.; Shen, G. Hierarchical Three-Dimensional $ZnCo_2O_4$ Nanowire Arrays/Carbon Cloth Anodes for a Novel Class of High-Performance Flexible Lithium-Ion Batteries. *Nano Lett.* **2012**, *12*, 3005−3011.
(10) Lavela, P.; Tirado, J. L. $CoFe_2O_4$ and $NiFe_2O_4$ synthesized by sol-gel procedures for their use as anode materials for Li ion batteries. *J. Power Sources* **2007**, *172*, 379−387.
(11) Cherian, C. T.; Sundaramurthy, J.; Reddy, M. V.; Kumar, P. S.; Mani, K.; Pliszka, D.; Sow, C. H.; Ramakrishna, S.; Chowdari, B. V. Morphologically Robust $NiFe_2O_4$ Nanofibers as High Capacity Li-Ion Battery Anode Material. *ACS Appl. Mater. Interfaces* **2013**, *5*, 9957−9963.
(12) Deng, Y.; Zhang, Q.; Tang, S.; Zhang, L.; Deng, S.; Shi, Z.; Chen, G. One-pot synthesis of $ZnFe_2O_4$/C hollow spheres as superior anode materials for lithium ion batteries. *Chem. Commun.* **2011**, *47*, 6828−6830.
(13) Sui, J.; Zhang, C.; Hong, D.; Li, J.; Cheng, Q.; Li, Z.; Cai, W. Facile synthesis of MWCNT-$ZnFe_2O_4$ nanocomposites as anode materials for lithium ion batteries. *J. Mater. Chem.* **2012**, *22*, 13674−13681.
(14) Teh, P. F.; Sharma, Y.; Pramana, S. S.; Srinivasan, M. Nanoweb anodes composed of one-dimensional, high aspect ratio, size tunable electrospun $ZnFe_2O_4$ nanofibers for lithium ion batteries. *J. Mater. Chem.* **2011**, *21*, 14999−15008.

DOI: 10.1021/acsomega.7b01752
ACS Omega 2018, 3, 2699−2705

(15) Bresser, D.; Paillard, E.; Kloepsch, R.; Krueger, S.; Fiedler, M.; Schmitz, R.; Baither, D.; Winter, M.; Passerini, S. Carbon Coated $ZnFe_2O_4$ Nanoparticles for Advanced Lithium-Ion Anodes. *Adv. Energy Mater.* **2013**, *3*, 513−523.
(16) Qi, Y.; Du, N.; Zhang, H.; Wu, P.; Yang, D. Synthesis of Co_2SnO_4@C core-shell nanostructures with reversible lithium storage. *J. Power Sources* **2011**, *196*, 10234−10239.
(17) Jiang, B.; Han, C.; Li, B.; Lin, Z.; et al. In-Situ Crafting of ZnFe(2)O(4) Nanoparticles Impregnated within Continuous Carbon Network as Advanced Anode Materials. *ACS Nano* **2016**, *10*, 2728−2735.
(18) Xue, D. J.; Xin, S.; Yan, Y.; Jiang, K. C.; Yin, Y. X.; Guo, Y. G.; Wan, L. J. Improving the Electrode Performance of Ge through Ge@C Core-Shell Nanoparticles and Graphene Networks. *J. Am. Chem. Soc.* **2012**, *134*, 2512−2515.
(19) Yao, X.; Zhao, C.; Kong, J.; Wu, H.; Zhou, D.; Lu, X. Dopamine-assisted one-pot synthesis of zinc ferrite-embedded porous carbon nanospheres for ultrafast and stable lithium ion batteries. *Chem. Commun.* **2014**, *50*, 14597−14600.
(20) Wei, W.; Yang, S.; Zhou, H.; Lieberwirth, I.; Feng, X.; Mullen, K. 3D Graphene Foams Cross-linked with Pre-encapsulated Fe_3O_4 Nanospheres for Enhanced Lithium Storage. *Adv. Mater.* **2013**, *25*, 2909−2914.
(21) Zhu, J.; Lei, D.; Zhang, G.; Li, Q.; Lu, B.; Wang, T. Carbon and graphene double protection strategy to improve the SnOx electrode performance anodes for lithium-ion batteries. *Nanoscale* **2013**, *5*, 5499−5505.
(22) Li, Y.; Zhang, H.; Shen, P. K. Ultrasmall metal oxide nanoparticles anchored on three-dimensional hierarchical porous graphene-like networks as anode for high-performance lithium ion batteries. *Nano Energy* **2015**, *13*, 563−572.
(23) Lee, S.; Cho, Y.; Song, H. K.; Lee, K. T.; Cho, J. Carbon-Coated Single-Crystal $LiMn_2O_4$ Nanoparticle Clusters as Cathode Material for High-Energy and High-Power Lithium-Ion Batteries. *Angew. Chem., Int. Ed.* **2012**, *51*, 8748−8752.
(24) Cai, J.; Wu, C.; Zhu, Y.; Shen, P. K.; Zhang, K. Hierarchical Porous Acetylene Black/$ZnFe_2O_4$@Carbon Hybrid Materials with High Capacity and Robust Cycling Performance for Li-ion Batteries. *Electrochim. Acta* **2016**, *187*, 584−592.
(25) Wang, M.; Ai, Z.; Zhang, L. Generalized Preparation of Porous Nanocrystalline $ZnFe_2O_4$ Superstructures from Zinc Ferrioxalate Precursor and Its Superparamagnetic Property. *J. Phys. Chem. C* **2008**, *112*, 13163−13170.
(26) Deng, Y.; Xu, H.; Bai, Z.; Huang, B.; Su, J.; Chen, G. Durable polydopamine-coated porous sulfur core-shell cathode for high performance lithium-sulfur batteries. *J. Power Sources* **2015**, *300*, 386−394.
(27) Fang, C.; Deng, Y.; Xie, Y.; Su, J.; Chen, G. Improving the Electrochemical Performance of Si Nanoparticle Anode Material by Synergistic Strategies of Polydopamine and Graphene Oxide Coatings. *J. Phys. Chem. C* **2015**, *119*, 1720−1728.
(28) Hao, L.; Wu, L.; Jia, Z.; Zhao, Y.; Li, X. Effects of polydopamine modification on self-grown CuO cube anodes in lithium-ion batteries. *Sci. China: Technol. Sci.* **2016**, *59*, 667−672.
(29) Lee, J. S.; Shin, M. S.; Lee, S. M. Electrochemical properties of polydopamine coated Ti-Si alloy anodes for Li-ion batteries. *Electrochim. Acta* **2016**, *222*, 1200−1209.
(30) Jiang, B.; He, Y.; Li, B.; Zhao, S.; Wang, S.; He, Y.; Lin, Z. Polymer-Templated Formation of Polydopamine-Coated SnO2 Nanocrystals: Anodes for Cyclable Lithium-Ion Batteries. *Angew. Chem., Int. Ed.* **2017**, *56*, 1869−1872.
(31) Wang, N.; Xu, H.; Chen, L.; Gu, X.; Yang, J.; Qian, Y. A general approach for MFe_2O_4 (M = Zn, Co, Ni) nanorods and their high performance as anode materials for lithium ion batteries. *J. Power Sources* **2014**, *247*, 163−169.
(32) Wang, Y.; Wang, S.; Niu, H.; Ma, Y.; Zeng, T.; Cai, Y.; Meng, Z. Preparation of polydopamine coated Fe_3O_4 nanoparticles and their application for enrichment of polycyclic aromatic hydrocarbons from environmental water samples. *J. Chromatogr. A* **2013**, *1283*, 20−26.
(33) Zhang, S.; Zhang, Y.; Bi, G.; Liu, J.; Wang, Z.; Xu, Q.; Xu, H.; Li, X. Mussel-inspired polydopamine biopolymer decorated with magnetic nanoparticles for multiple pollutants removal. *J. Hazard. Mater* **2014**, *270*, 27−34.
(34) Wang, Y.; Zhang, Y.; Hou, C.; Liu, M. Mussel-inspired synthesis of magnetic polydopamine-chitosan nanoparticles as biosorbent for dyes and metals removal. *J. Taiwan Inst. Chem. Eng.* **2016**, *61*, 292−298.
(35) Knorr, D. B., Jr.; Tran, N. T.; Gaskell, K. J.; Orlicki, J. A.; Woicik, J. C.; Jaye, C.; Fischer, D. A.; Lenhart, J. L. Synthesis and Characterization of Aminopropyltriethoxysilane-Polydopamine Coatings. *Langmuir* **2016**, *32*, 4370−4381.
(36) Yue, H.; Wang, Q.; Shi, Z.; Ma, C.; Ding, Y.; Huo, N.; Zhang, J.; Yang, S. Porous Hierarchical Nitrogen-doped Carbon Coated $ZnFe_2O_4$ Composites as High Performance Anode Materials for Lithium Ion Batteries. *Electrochim. Acta* **2015**, *180*, 622−628.
(37) Peng, S.; Li, L.; Mhaisalkar, S. G.; Srinivasan, M.; Ramakrishna, S.; Yan, Q. Hollow Nanospheres Constructed by CoS_2 Nanosheets with a Nitrogen-Doped-Carbon Coating for Energy-Storage and Photocatalysis. *ChemSusChem* **2014**, *7*, 2212−2220.
(38) Cao, Y.; Zhang, L.; Tao, D.; Huo, D.; Su, K. Facile synthesis of $CoSnO_3$/Graphene nanohybrid with superior lithium storage capability. *Electrochim. Acta* **2014**, *132*, 483−489.
(39) Lin, L.; Pan, Q. $ZnFe_2O_4$@C/graphene nanocomposites as excellent anode materials for lithium batteries. *J. Mater. Chem. A* **2015**, *3*, 1724−1729.
(40) Park, S. H.; Kim, H. J.; Lee, J.; Jeong, Y. K.; Choi, J. W.; Lee, H. Mussel-Inspired Polydopamine Coating for Enhanced Thermal Stability and Rate Performance of Graphite Anodes in Li-Ion Batteries. *ACS Appl. Mater. Interfaces* **2016**, *8*, 13973−13981.
(41) Yuan, C.; Cao, H.; Zhu, S.; Hua, H.; Hou, L. Core-shell ZnO/$ZnFe_2O_4$@C mesoporous nanospheres with enhanced lithium storage properties towards high-performance Li-ion batteries. *J. Mater. Chem. A* **2015**, *3*, 20389−20398.
(42) Wang, Q.; Yue, H.; Du, T.; Zhang, W.; Qiao, Y.; Dong, H.; Yin, Y.; Yang, S. A particle-carbon matrix architecture for long-term cycle stability of $ZnFe_2O_4$ anode. *RSC Adv.* **2016**, *6*, 35110−35117.
(43) Thankachan, R. M.; Rahman, M. M.; Sultana, I.; Glushenkov, A. M.; Thomas, S.; Kalarikkal, N.; Chen, Y. Enhanced lithium storage in $ZnFe_2O_4$-C nanocomposite produced by a low-energy ball milling. *J. Power Sources* **2015**, *282*, 462−470.
(44) Shi, J.; Zhou, X.; Liu, Y.; Su, Q.; Zhang, J.; Du, G. One-pot solvothermal synthesis of $ZnFe_2O_4$ nanospheres/graphene composites with improved lithium-storage performance. *Mater. Res. Bull.* **2015**, *65*, 204−209.

DOI: 10.1021/acsomega.7b01752
ACS Omega 2018, 3, 2699−2705